Dynamic behavior of nuclear shape induced by visual stimulation in excitatory neurons of visual cortex

Tanita Frey[1,2], Tomonari Murakami[3,4], Kenichi Ohki[3,4,5], Yukiko Gotoh[1,5]*, and Yusuke Kishi[1,6]*

[1]Graduate School of Pharmaceutical Sciences, The University of Tokyo, 7-3-1 Hongo, Bunkyo-ku, Tokyo 113-0033, Japan.
[2]New York University Grossman School of Medicine, New York NY, 10016, United States
[3]Graduate School of Medicine, The University of Tokyo, 7-3-1 Hongo, Bunkyo-ku, Tokyo 113-0033, Japan.
[4]Institute for AI and Beyond, The University of Tokyo, 7-3-1 Hongo, Bunkyo-ku, Tokyo 113-0033, Japan
[5]International Research Center for Neurointelligence (WPI-IRCN), The University of Tokyo, 7-3-1 Hongo, Bunkyo-ku, Tokyo 113-0033, Japan
[6]Institute for Quantitative Biosciences, The University of Tokyo, 1-1-1 Yayoi, Bunkyo-ku, Tokyo 113-0032, Japan.

*Correspondence: ygotoh@mol.f.u-tokyo.ac.jp (Y.G.), ykisi@iqb.u-tokyo.ac.jp (Y.K.)

Abstract

External stimuli contribute to the neuronal properties partly through regulating gene expression. Previous works have shown nuclear infolding induced by external stimuli and pathological conditions in neurons. However, the dynamics and reversibility of the changes in nuclear shape upon external stimuli have been unknown. In this study, we found that the nuclear shape of excitatory neurons in the visual cortex altered and undergo invagination upon visual stimuli. Subsequently, we performed time-lapse imaging of the nuclear shape of excitatory neurons in the visual cortex using *Nex-Cre;SUN1-GFP* mice, labeling the nuclear membrane of excitatory neurons with GFP. We found that nuclear infolding can be observed within the first 15 minutes of light exposure. Depletion of the stimuli by finishing the light exposure or injection of MK-801, an inhibitor of NMDA receptor, restored the nucleus to a spherical shape and reduced the dynamic behavior, suggesting that nuclear infolding in neurons is reversible process. Then, as brain function declines naturally over age, we also examine the nuclear shapes of neurons in aged mice. In contrast to young mice, the nuclear shape in aged mice showed less dynamic change upon light stimulation. In conclusion, our data highlights the changes of the nuclear shape upon visual stimulation and its potential role in the response towards external stimuli and the dysfunction of the aged brain.

Introduction

The brain consists of a wide neuronal network, and for any information to be transmitted, neurons require either internal or external stimuli. Since external factors are able to induce morphological changes in neurons, such as in their axon, dendrites, and synapses (Greer and Greenberg, 2008; Wong and Ghosh, 2002), the responsiveness to external stimuli is critical for the neuronal plasticity of the brain functions, such as memory formation.

Associated with the remodeling of transcriptome upon a neuronal activity (Flavell and Greenberg, 2008), neuronal nuclei change their shape upon external stimuli. In the neuronal culture of the hippocampus and dorsal thalamus, neuronal activity induced via blocking GABA receptors using bicuculline increased the portion of the infolded nuclei marked by their invaginated nuclear membrane (Chen et al., 2020; Feurle et al., 2020; Wittmann et al., 2009). Also, the physiological stimulation by exposure to an enriched environment increased the amount of infolded nuclei in the CA1 of the hippocampus (Feurle et al., 2020). Nuclear infolding in neurons is implicated in playing a role in regulating gene transcription and nuclear compartmentalization. The neurons with infolded nuclei tended to have more phosphorylated histone H3 at serine 10, a histone modification for gene activation (Wittmann et al., 2009). Also, Satb2, a neuronal transcription factor, is involved in inducing the infolding of neuronal nuclei (Feurle et al., 2020). Additionally, multiple nuclear compartments separated by invagination of nuclear membrane presented different amounts of calcium signaling (Wittmann et al., 2009).

On the other hand, nuclear infolding is suggested to be involved in the defective condition of brains. In human patients with Parkinson's disease (PD), neuronal nuclei are rather infolded than spherical shape in the hippocampus, the frontal cortex, and the substantia nigra (Liu et al., 2012; Shani et al., 2019). This finding was further supported by works on the PD-model mice, knockout or G2019S point mutation of the Lrrk2 kinase, in which the nuclei in substantia nigra and dorsal thalamus showed more infolded nuclei (Chen et al., 2020; Shani et al., 2019). Similar infolded nuclear shapes in neurons were found in the mouse model and human patients with Huntington's disease (HD) (Alcalá-Vida et al., 2021). In consideration that neuronal nuclei from a mouse model of HD or Lrrk2 G2019S transgenic mouse showed a higher permeability of nuclear membrane (Alcalá-Vida et al., 2021; Shani et al., 2019), the role of nuclear infolding can be interpreted as positive and negative depending on the context of those morphological change occurrences. Taken together, these studies indicate the role of nuclear infolding in regulating neuronal function, such as gene expression upon neuronal activity and defects in cytoplasmic-nuclear transport in some neurological diseases; however, the significance remains unknown.

In order to get closer to the understanding of nuclear infolding and its role in the neuronal context, it is necessary to examine the dynamics of the nuclear

shape upon external stimuli in the physiological condition. In this study, we analyzed the nuclear shape of excitatory neurons in the visual cortex upon light stimulation after dark rearing and confirmed the increased number of infolded nuclei. To further reveal the dynamics of the infolding process, we performed time-lapse imaging of the nuclear shape of excitatory neurons in the upper layer of the visual cortex of *Nex-Cre;SUN1-GFP* transgenic mice, whose nuclei in excitatory neurons were labeled with GFP fused with SUN1 outer nuclear membrane protein (Goebbels et al., 2006; Mo et al., 2015). Over the course of light stimulation, nuclear shapes in the excitatory neurons of the visual cortex showed dynamic changes toward an infolded morphology, which was observed 15 min after visual cue exposure. After turning off the light stimulation, the nuclei's dynamics turned down and spherical shape reappeared similarly to conditions before the light stimulation, suggesting reversible changes of the nuclear morphology. Additionally, we also examined nuclear infolding in the context of aging as a condition of the natural decline of brain function. The aged visual cortex (over two-year-old) before the visual stimulation already showed a higher portion of infolded nuclei than spherical ones. Time-lapse imaging of aged mice revealed that the nuclei were less dynamic compared to young mice and showed less morphological responses towards the exposure to stimulation. In our research, we first presented the temporal output of visual stimulation on the nuclear shape in the visual cortex of excitatory neurons. Those dynamic changes of morphology on the nuclear shape indicate their crucial role in neuronal functions.

Results

Light stimulation after conditional enucleation and dark rearing induces the expression of immediate early genes (IEGs) in the visual cortex

Previous studies have examined the changes in nuclear shape via different evoked stimulation systems (Chen et al., 2020; Feurle et al., 2020; Wittmann et al., 2009). To tackle the *in vivo* nuclear shape behavior in relation to neuronal activity upon physiological stimulation, we utilized the visual system due to its simplified manipulative approach via ocular enucleation and dark rearing. First, we confirmed the manipulation of neuronal activity in dependence on the ocular enucleation in the visual cortex of mice. Thereby, we performed enucleation of the left (monocular) or both eyes of *ICR* wild-type male mice of an age of 6 weeks. After the enucleation, the mice were exposed to five days of dark rearing to reduce the neuronal activity in the visual cortex to a baseline (Lyckman et al., 2008). These mice were followed by 4 hours of light exposure, and the visual cortices were subjected to RT-qPCR analysis for *Npas4*, which is a representative IEGs induced by neuronal activity (Supplementary Fig. 1A, B). Visual cortices from mice with no enucleation, two intact eyes, or left visual cortex from monocular-deprived mice presented higher IEGs expressions compared to visual cortices from mice with enucleation of both eyes or right visual cortex from the monocular-deprived mouse. Based on this result, we were able to confirm that enucleation and light exposure after dark rearing stimulates the visual cortex.

Infolding of nuclear shape within excitatory neurons increases upon visual stimulation in the visual cortex

Using the prior established visual manipulation, we aim to examine the nuclear shape in excitatory neurons of the visual cortex in *NexCre;SUN1-GFP* mice which express the GFP-fused SUN1 protein, a protein on the outer nuclear membrane, under the control of *NeuroD6/Nex* gene locus (Goebbels et al., 2006; Mo et al., 2015). We enucleated the left eye of 6- to 9-week-old *NexCre;SUN1-GFP* mice, harvested them in a dark room for five days, and exposed them to the light for 4 hours (Fig. 1A). The brain slices were immunostained with the antibodies to GFP and c-Fos for evaluating the neuronal activity (Fig. 1B). The left (light stimulated) hemispheres showed an increase in their c-Fos expression in comparison to the right (light deprived) hemisphere in the visual cortex (Fig. 1B, D), again supporting the notion that our dark rearing of monocular mice and light stimulation appropriately manipulate the neuronal activity. The GFP staining pattern showed spherical or infolded nuclear shapes (Fig. 1B), and their numbers were counted within the stimulated and deprived hemisphere of monocular enucleated mice (Fig. 1C). In the left hemisphere, the nuclear shape distribution showed a strong dominance of infolded nuclei (79%) in comparison to spherical ones (21%). In contrast, infolded nuclei were less (59%) in the right hemisphere. Moreover, most

of the infolded nuclei in the left hemisphere were c-Fos-positive, suggesting that physiological visual stimulation induces the nuclear infolding in the visual cortex.

Since the distinguishment of nuclear shapes has relied on the subjective observations of the SUN1-GFP signal, we next evaluated the nuclear shape using two objective values, circularity and area ratio. Previous studies have evaluated nuclear infolding by reduction of circularity value (Alcalá-Vida et al., 2021; Chen et al., 2020). We examined the circularity value of the inner area of the SUN1-GFP signal (a gray area in Fig. 1D) and found that circularity in the left visual cortex was lower than that in the right one (Fig. 1E). We also defined the area ratio value; the SUN1-GFP signal area divided by the non-SUN1-GFP occupied area within the nucleus (Fig. 1D). This means that a higher area ratio value represents a more infolded or invaginated nuclear shape. When we examined the area ratio value in the left visual cortex, it turned out to be higher than that in the right one (Fig. 1F). Therefore, these results suggest that the neuronal activity by light stimulation induced the shift of nuclear shapes towards an infolded shape within excitatory neurons of the visual cortex.

The nuclear shape of excitatory neurons dynamically changes in response to visual stimulation in vivo

In consideration that nuclear infolding can be observed upon exposure to visual stimulation in excitatory neurons within the visual cortex, it raises the question of the infolding process and its temporal relationship to neuronal activity. Therefore, we performed live imaging of the upper layer of the visual cortex in *NexCre;SUN1-GFP* mice *in vivo* with two-photon microscopy during visual light exposure following the prior preparations of craniotomy on the visual cortex for time-lapse imaging (Fig. 2A*)*. After the AAV injection, the mice were recovered for more than two weeks and harvested in a dark room for five days. Then, we set them up in front of a black monitor with the black image under anesthesia for the “before light stimulation” recordings for around one hour. For visual stimulation, the mice were exposed to spatially randomized visual cues presented on the monitor separated by four seconds grey screen presentations. Around 20 min imaging of SUN1-GFP signals before the light stimulation showed a stable and spherical nuclear shape of excitatory neurons in the upper layer (Fig. 2B). However, the nuclear shape changed dynamically and became infolded during the light stimulation (Fig. 2B). We classified the nuclear shapes into changed or maintained and spherical or infolded before and during the exposure to light stimulation (Fig. 2C). We found that most of the nuclei before stimulation (50%) maintained their spherical shape, while 37% of the nuclei during stimulation changed their nuclear shape from spherical to infolded.

In the following, we evaluated the nuclear shape using the area ratio value defined in Fig. 1D. Before light stimulation, the area ratio did not change for 20 min of non-light exposure (Fig. 3A). However, during light stimulation, the area

ratio started to increase after the first 15 min of exposure (Fig. 3B). This suggests that the nuclear shapes of excitatory neurons in visual cortex require around 15 min to start altering their shape upon visual stimulation.

Dynamic behavior in nuclear shapes decreases after inhibiting neuronal activity in excitatory neurons

The strong relationship of neuronal activity to nuclear shape raises another question; what would happen to the nuclear shape once the neuronal activity is inhibited? First, we examined the changes in SUN1-GFP patterns after turning off the visual stimulation by changing to the black image on the monitor. During the first 20 min, the dynamic behavior of nuclear shapes gradually decreased and became similar to the area ratio value as before stimulation at 25 min (Fig. 3C), suggesting that the nuclear shape takes around 20 min to turn down the dynamics observed during stimulation.

Additionally, we also examined the effect of inhibiting neuronal activity by another method, pharmacological inhibition of calcium influx. MK-801 is an antagonist to the NMDA receptor, and its administration reduces the calcium influx and neuronal activity. To assure that MK-801 interferes with the neuronal activity, C57BL6/J wild-type female mice at six weeks of age were analyzed for the expression pattern of IEGs. Following the five days of dark rearing treatment, the mice were exposed to 2 h of light and then injected with MK-801. RT-qPCR analysis of the visual cortex showed the weakened expression of *c-Fos* in MK-801 injected brains compared to saline-injected ones; thus, confirming the effect of MK-801 on the neuronal activity induced by the visual stimulation (Supplementary Fig. 2A). On this basis, we performed time-lapse imaging of *NexCre;SUN1-GFP* mice with MK-801 injection onto the visual cortex following two hours of light exposure; we examined the response of the nuclear shape upon the NMDA inhibitor application while presenting visual cues. We imaged the visual cortex around one hour after injection and found that the nuclear shapes decreased their area ratio despite the presence of light stimulation. (Fig. 3D). These results suggest that the NMDA activation and the calcium influx in excitatory neurons of the visual cortex are necessary for the dynamic changes in nuclear shape.

Taken together, these results indicate that the dynamic behavior of nuclear shapes induced by neuronal activity is a reversible event in an in vivo physiological system. Consistent with this result, the previous study showed that inhibition of neuronal activity by treating with tetrodotoxin (TTX) in a hippocampal neuronal culture decreases the infolded nuclei (Wittmann et al., 2009).

The nuclei in aged mice are more infolded and have less dynamic behavior compared to those in young mice

In addition to the neuronal activity-induced nuclear infolding, previous studies have shown more infolded nuclei in human patients and model mice of PD and HD (Alcalá-Vida et al., 2021; Liu et al., 2012; Shani et al., 2019). Since both PD and HD are aging-associated neurodegenerative diseases, we next examined the shape and dynamics of the nuclei in aged mice. We prepared 7-week-old and 133-week-old *C57BL6/J* wild-type mice and performed left eye enucleation and five days of dark rearing (Fig. 4A). Upon collecting the brains, their slices were immunostained with the antibodies for c-Fos and Lamin B1, a component of the inner nuclear membrane (Fig. 4B). c-Fos staining confirmed the appropriate stimulation for the cells in the left visual cortex, not in the right visual cortex. In the young brain, the nuclear shape observed by Lamin B1 exhibited more infolded than spherical morphology in the left brain compared to the right brain (Fig. 4B, C). However, the nuclear shapes in aged mice demonstrated an overall infolded appearance regardless of left or right condition (Fig. 4B, C). Also, the infolded nuclear state in the right brain of aged mice was evaluated by circularity and area ratio analysis (Fig. 4D, E), and it reveals nuclear shapes presenting a resting infolded state independent of any stimulation in the aged brain. Therefore, this result suggests that neuronal aging induces nuclear infolding resembling the prior observed nuclear shapes in PD and HD brains (Alcalá-Vida et al., 2021; Chen et al., 2020; Shani et al., 2019); leading to the assumption that defective conditions of the brain may be associated with infolded shapes of neuronal nuclei.

As priorly in young mice, we investigated the temporal dynamics of aged nuclei. Therefore, we performed time-lapse imaging of nuclear shape in upper layer neurons using aged *Nex-Cre;SUN1-GFP* mice as in Fig. 2 (Fig. 5A). Similar to the immunohistochemistry data (Fig. 4), we found that more nuclei presented infolded shape and the area ratio value was higher in aged mice compared to young mice even before stimulation (Fig. 5 B, C). Additionally, the nuclear shape did not alter during stimulation and maintained a stable area ratio value throughout the imaging (Fig. 5 B, C). The lack of nuclear shape alteration in excitatory neurons toward visual stimulation in aged mice suggests that the dynamics of nuclei morphology change with age.

Discussion

Nuclear infolding upon a neuronal activity or in a defective condition of neurons has been observed in previous papers, but its regulatory mechanism and significance have not been fully understood. In this study, we found that an in vivo physiological stimulation, light stimulation for the visual cortex, induced nuclear infolding in excitatory neurons. Furthermore, time-lapse imaging of the nuclear shape of excitatory neurons in the upper layer showed the dynamic behavior of the nucleus during light stimulation. The treatment with MK-801 reduced the dynamic behavior as in the previous study using hippocampal slice culture (Wittmann et al., 2009). This suggests that calcium influx mediated by the NMDA receptor is upstream of nuclear infolding. In our imaging analysis, it takes around 15 min to start dynamic behavior of the nucleus after light stimulation. A previous study using hippocampal neuronal culture has shown the involvement of MAP kinase signaling in this process since MEK inhibitors, such as PD98059 and U0126, inhibited neuronal activity-dependent nuclear infolding (Wittmann et al., 2009). Upon KCl stimulation, MAP kinase, such as Erk, becomes phosphorylated and activated within 5 min (Tyssowski et al., 2018). This is consistent with the idea that dynamic behavior and infolding of a neuronal nucleus are mediated by MAP kinase.

External stimuli induce transcription of several genes in neurons and have an important role in the functional changes of neurons, such as neurite and synapse formation (Flavell and Greenberg, 2008; Greer and Greenberg, 2008). Among these induced genes, a gene set called IEGs or rapid PRGs, including *c-Fos* and *Arc*, increased their expression levels within 20 min upon visual stimulation and decreased after turning off the stimulation (Tyssowski et al., 2018). This time course and reversibility are similar to the induction of nuclear infolding observed in the time-lapse imaging of this study. Considering that the components of the inner nuclear membrane, such as Lamin, are involved in gene transcription through regulating chromatin structure, the changes in the nuclear shape may contribute to the regulation of gene transcription. This is further supported by the previous work studying the role of the interaction between Satb2, a neuronal transcription factor, and Lemd2, a component of the inner nuclear membrane (Feurle et al., 2020). Then, how does nuclear infolding contribute to gene induction? One possibility is that the nuclear infolding may allow the rapid interactions between IEG genomic loci and their regulatory elements. Previous Hi-C experiment using hippocampal neurons after the kainic acid injection has shown the chromatin interactions at the gene loci of responsive genes, such as *c-Fos* and *BDNF*, within one hour (Fernandez-Albert et al., 2019). In contrast, the interaction between the nuclear membrane and the responsive gene loci, such as *Egr3* and *BDNF*, visualized by FISH, has not altered after bicuculline treatment in hippocampal neuronal culture (Noguchi et al., 2021). Therefore, the nuclear

membrane may require to be infolded in order for the regulatory element to interact with the gene loci while still bound to the nuclear membrane.

In the aged visual cortex over two years old, the nuclei of excitatory neurons generally demonstrated a higher portion of infolded nuclei than the young visual cortex in non-stimulated conditions. In the previous study, invagination of the nuclei of spiny projection neurons in striatal in wild-type mice did not increase in aged mice (two-year-olds) compared to young (two-month-old) (Chen et al., 2020). This discrepancy may be caused by the difference in the neuronal type, the brain area, and the harvesting condition of mice. Then, what is the cause for the higher population of infolded nuclei in aged excitatory neurons? Long-term stimulation (40 h) of hippocampal neurons by bicuculline induces a more stable infolded nuclear shape after TTX treatment compared to short-term stimulation (1 h) (Wittmann et al., 2009). This suggests that more stimulation induces the fixed nuclear-infolded shape. Aged excitatory neurons have naturally undergone repeated neuronal activity exposure and thus, may cause the irreversible infolded nuclear shape and the dysfunction of neuronal nuclei. Consistently, our time-lapse imaging of nuclei of aged excitatory neurons revealed a decrease in dynamic behavior compared to those of young ones.

More infolded nuclear shape in the aged visual cortex in this study is similar results to the nuclear shape in PD and HD (Alcalá-Vida et al., 2021; Liu et al., 2012; Shani et al., 2019). Since both PD and HD are aging-associated neurodegenerative disorders, our results indicate that increase of infolded nuclei is associated with the decline of neuronal functions. Previous studies have shown the leakiness of the nuclear membrane of infolded nuclei is higher than that of spherical nuclei (Alcalá-Vida et al., 2021; Shani et al., 2019) and suggest that defects in cytoplasmic-nuclear transport of proteins occur in aged neurons. In another study, micropipette aspiration of the nuclear membrane of embryonic stem cells (ESCs), differentiated neural progenitor cells, and tissue fibroblast revealed a more deformable nuclear membrane of ESCs compared to differentiated cells (Pajerowski et al., 2007). ESCs have more plasticity for lineage choice and gene transcription (Meshorer and Misteli, 2006). Therefore, it is supposed that deformable nuclear membrane contributes to plasticity. Younger neurons also have more plasticity and adapt easier to functional changes (Berardi et al., 2000; Katz and Crowley, 2002). Therefore, less dynamic behavior of nuclear shape in aged neurons may be related to their decrease of plasticity through regulating the events induced by neuronal activity, such as induction of IEGs.

357 **Material and Methods**
358
359 **Animals.**
360 ICR or C57BL/6J mice (Japan CREA) were used for the study of wild-type mice.
361 *Nex-Cre* mice were provided by Klaus-Armin Nave (Max Planck Institute), and
362 *SUN1-GFP* mice (#021039) were obtained from The Jackson Laboratory. The
363 age of the mice is indicated in Figure legends. All mice were maintained in a
364 temperature- and relative humidity–controlled (23° ± 3 °C and 50 ± 15%,
365 respectively) environment with a normal 12-h-light, 12-h-dark cycle. They were
366 housed in two to six per sterile cage (Innocage, Innovive; or Micro BARRIER
367 Systems, Edstrom Japan) with chips (PALSOFT, Oriental Yeast; or PaperClean,
368 SLC Japan), and irradiated food (CE-2, CLEA Japan) and filtered water available
369 ad libitum. All animals were maintained and studied according to protocols
370 approved by the Animal Care and Use Committee of The University of Tokyo.
371
372 **Enucleation and dark rearing in mice for neuronal activity manipulation.**
373 The eye removal was performed under 2% isoflurane. The mouse was placed on
374 a little pedestal. A tweezer clipped the optical nerve behind the eye, and then the
375 eye was removed. The wound was glued via tissue adhesive application from
376 Vetbond. After the left eye removal and the mice's recovery, they were exposed
377 to 5 days of darkness within a box which is covered by a dark sheet to get the
378 neuronal activity of the visual cortex to its lowest baseline.
379
380 **RT-qPCR analysis.**
381 The visual cortex was dissected with a stainless steel 0.5 mm sagittal brain matrix
382 for rodents. The brain was firstly cut at 1.5 mm and 3.5 mm from the midline.
383 Then, the visual cortex was located over one-third of the posterior part of the
384 hippocampus. The dissected visual cortex was put into RNAiso plus (Takara),
385 and total RNA was precipitated according to the manufacturer's protocol. The
386 amounts of obtained RNA were measured via NanoDrop One, Thermo Scientific,
387 and 0.5 μg of the RNA was subjected to reverse-transcription with the use of
388 ReverTra Ace qPCR RT Master Mix with gDNA Remover (Toyobo) according to
389 the manufacturer protocol. The resulting cDNA was subjected to real-time PCR
390 analysis in a LightCycler 480 instrument (Roche) with Thunderbird SYBR qPCR
391 mix (Toyobo). The amount of each target mRNA was normalized by that of *Actb*
392 or *GAPDH* mRNA. Primer sequences are provided in Supplementary Table 1.
393
394 **Immunohistochemistry**
395 Immunohistochemistry was performed as previously described (Eto et al., 2020).
396 mice have intraperitoneally injected with anesthesia Penotobarbital (Nakarai
397 tesque) solution. Cold PBS was flushed via a 30G needle, followed by clod 4%
398 paraformaldehyde (PFA) in phosphate-buffered saline (PBS) on the left heart
399 ventricle. After perfusion, the brains were removed and soaked overnight in 4%

PFA on a rotator, and then they were incubated with 10%, 20%, and 30% sucrose in PBS and embedded with O.C.T. compound (Sakura Finetek Japan) at –80°C. 16 μm coronal sections of embedded brains were prepared by a cryostat. For staining, samples were exposed to antigen retrieval (10 min at 105°C in 1 x TRS (DAKO)). Then the samples were exposed to Tris-buffered saline containing 0.1% Triton X-100 and 3% bovine serum albumin (blocking buffer) for two h at room temperature, incubated first overnight at four °C with primary antibodies, listed in Supplementary Table 2, in blocking buffer and then for two h at room temperature with Alexa Fluor–conjugated secondary antibodies (1: 1000, Thermo Fisher Scientific) in blocking buffer, and mounted in Mowiol (Calbiochem). All images were taken by Leica SP5 or Zeiss LSM 880.

Craniotomy and viral injection into the visual cortex.

Nex-Cre;SUN1-GFP mice were prepared for in vivo imaging as described previously (Murakami et al., 2015; Ohki and Reid, 2014). Under stereotaxis conditions, which were performed under constant 2% isoflurane exposure. The skin over the skull was removed, and any muscle in proximity was cleanly cut off to ensure a dry area on which the plate could be positioned and glued by the Super-bond dental cement (Sun Medical). A custom-made metal head plate was glued on the skull, and the area of interest was located at the caudal region around 4 mm from Lambda in the partial bone – the visual cortex. The craniotomy was made over the entire visual cortex, and the dura (thin protective layer on the brain) was carefully removed. 500 nl of the virus, AAV1-Syn-Flex-NES-jRGECOSa-WPRE-SV40 (Plasmid #100854, Addgene) (Dana et al., 2016), in saline was directly injected into the cortex at a speed of 1 nl/sec by Nanoject III (Drummond), while covered by artificial CSF. Afterward, the window was closed with glass slips (5.5 mm and 4 mm glued onto each other) and the use of clear glue and dental cement (ADFA, Shofu Inc). The closed window was further covered for protection with dental silicone (Shofu Inc). After around two weeks, the window was checked for its clearness and covered again with the dental silicone. Five days prior to the recordings, the mice were put into a dark rearing box.

Microinjection of inhibitor.

The skin was opened and removed to insert a pinhole with a 30G needle onto the visual cortex (the caudal region around 4 mm from Lambda in the partial bone) in mice under 2% isoflurane anesthesia in stereotaxis fixation. 500 nl of 100 mM MK-801 in saline was injected at a speed of 1 nl/sec into the left hemisphere by the Nanoject III [35,65] (as prior observed by Medeiros et al., 2014). The right visual cortex, as a control, got saline injected. The skin was stitched close after injection.

Two-photon microscopy of the visual cortex of *Nex-Cre;SUN1-GFP* mice.

After around two weeks from the craniotomy, the mice were exposed to darkness for five days in a dark rearing box and seated on a heat block during the entire time of recording. During anesthetized recordings, mice were sedated with chlorprothixene (0.3–0.8 mg/kg; Sigma-Aldrich) and isoflurane (0.8%). The recordings were done with NIS-Elements AR (Nikon) using a two-photon microscope (Nikon A1MP) equipped with a mode-locked Ti:sapphire laser (Mai Tai Deep See; Spectra Physics). The excitation light was focused with a 25x objective (Nikon Plan Apo, NA 1.10). GFP and jRGECO signals were excited at 960 nm, and the emission was filtered at 517–567 nm and 570–625 nm, respectively. A square region of the cortex (512 x 512 pixels, ~330 μm on a side) was imaged at 2 frames/min. Images were obtained from layers 2/3 (200–300 μm from the pia). Visual stimuli were generated by using custom-written programs in PsychoPy (Peirce, 2007). The stimulus presentation was synchronized with the frame acquisition of images using a counter board (NI USB-6501; National Instruments). We positioned a 32-inch LCD monitor 18 cm from the right eye of each mouse. Drifting rectangle strips of different angles were presented as wave gratings in randomized manner. For the conversion of the recordings, Matlab R2020b (version 4 9.9) was used. Note that we did not use the jRGECO signals for further analysis because of insufficient image quality.

Statistical analysis. Data are presented as means +s.d. and were compared with the two-tailed Student's paired or unpaired *t*-test or by analysis of variance (ANOVA) followed by Tukey's multiple-comparison test. P value of < 0.05 was considered as statistically significant.

Acknowledgments

We thank Klaus-Armin Nave (Max Planck Institute) for providing *Nex-Cre* mice; Jeremy Nathans (John Hopkins Medical School) for providing *SUN1-GFP* mice. E. Ogawara for technical assistance; and members of the Gotoh laboratory for discussion. This research was supported by MEXT Scholarship for T.F. AMED-CREST (22gm1310004 to Y.G.), AMED-PRIME (JP22gm6110021 to Y.K.), by MEXT/JSPS KAKENHI (22H00431 to Y.G.; 20H03179, 21H00242, 22K19823, and JP16H06279 to Y.K.) grants, by Takeda Science Foundation, by Mochida Memorial Foundation for Medical and Pharmaceutical Research, and by SECOM Science and Technology Foundation.

Author contributions

T.F., Y.G., and Y.K. designed the study and wrote the manuscript. T.F., T.M., and Y.K. performed the experiments and analyzed the data. T.M. and K.O. helped for time-lapse imaging. Y.G. and Y.K. supervised the study. All authors contributed to the revision and approved the final version of the manuscript.

Competing interests

The authors declare no competing interests.

490 **Figure legends**
491
492 **Figure 1. Nuclear infolding in the excitatory neurons in the primary visual**
493 **cortex induced by visual stimulation.**
494 **(A)** Left eyes of 6- to 9-week-old *Nex-Cre;SUN1-GFP* mice were enucleated, and
495 the mice were harvested in a dark room for five days. They were stimulated by
496 room light for four hours and subjected to immunohistochemistry. **(B)** Coronal
497 sections of the brain were stained with antibodies to c-Fos and GFP. Nuclei were
498 counterstained with Hoechst 33342. The images were obtained from layer 2/3 of
499 the primary visual cortex. Arrows and arrowheads indicate infolded and spherical
500 nuclei, respectively. Scale bars, 20 μm. **(C)** Quantification of the proportion of c-
501 Fos-positive and spherical or infolded nuclear shape among all GFP-positive cells
502 in all layers of the primary visual cortex. **(D)** Area ratio values were determined
503 as the area of GFP signals divided by the inside area after binarization of the
504 nuclear image. (**E, F**) Quantification of circularity (E) or area ratio (F) value of
505 SUN1-GFP signals in the left and right visual cortex. 81 to 101 nuclei from two
506 independent experiments were analyzed.
507
508 **Figure 2. Time-lapse imaging of nuclear shape of the excitatory neurons in**
509 **the primary visual cortex upon visual stimulation.**
510 **(A)** 6- to 9-week-old *Nex-Cre;SUN1-GFP* mice were subjected to craniotomy for
511 time-lapse imaging. After recovering for around two weeks and being harvested
512 in the darkroom for five days, the mice were set on the two-photon microscopy in
513 front of the monitor. The nuclear shape visualized by GFP in layer 2/3 was
514 recorded in the interval of 0.5 min with the black image ("Before") and then with
515 the stripe image ("During"). **(B)** Representative images of GFP signals in “before”
516 (upper two panels) and “during” (lower two panels) conditions. Arrows indicate
517 invaginated area after recording. Scale bars, 2 μm. **(C)** Quantification of the
518 proportion of the nuclei showing the “maintained” or “changed” shape between
519 spherical and infolded during the recording are shown. Three hundred thirty-two
520 nuclei in "before" and 305 nuclei in "during" from 5 independent experiments were
521 analyzed. Data are means +s.d. *$p < 0.05$, *$p < 0.01$ (two-tailed Student's paired
522 t-test).
523
524 **Figure 3. The behavior of the nuclear shape before, during, and after visual**
525 **stimulation.**
526 **(A, B)** Quantification of area ratio values at indicated time in “before” (A) or “during”
527 (B) recording. **(C, D)** Experimental schemes and quantification of area ratio
528 values at indicated time in “after” (C) or “MK-801” (D) recording. Fifty-two nuclei
529 from 5 independent experiments (A), 38 nuclei from 5 independent experiments
530 (B), 25 nuclei from 3 independent experiments (C), and 30 nuclei from 3
531 independent experiments (D) were analyzed. Data are means +s.d. *$p < 0.05$, *p

532 < 0.01, n.s., not significant (one-way ANOVA followed by Tukey's multiple-
533 comparison test).
534
535 **Figure 4. More infolded nuclei in the excitatory neurons in the aged primary**
536 **visual cortex without visual stimulation.**
537 **(A)** Left eyes of 7- or 133-week-old *C57BL6/J* wild-type mice were analyzed as
538 in Fig. 1A **(B)** Coronal sections of the brain were stained with the antibodies to c-
539 Fos and Lamin B1. Nuclei were counterstained with Hoechst 33342. The images
540 were obtained from layer 2/3 of the primary visual cortex. Scale bars, 20 μm. **(C)**
541 Quantification of the proportion of c-Fos-positive and spherical or infolded nuclear
542 shape in all layers of the primary visual cortex. (**D, E**) Quantification of circularity
543 (D) or area ratio (E) value of Lamin B1 signals in the left and right visual cortex of
544 young and aged mice. 126 to 202 nuclei from two independent experiments were
545 analyzed. Data are means +s.d. *$p < 0.05$, *$p < 0.01$ (one-way ANOVA followed
546 by Tukey's multiple-comparison test).
547
548 **Figure 5. Less dynamic behavior of the nuclear shape in the aged brain**
549 **(A)** More than 98-week-old *Nex-Cre;SUN1-GFP* mice were analyzed as in Fig.
550 2A. **(B)** Representative images of GFP signals in "before" (upper two panels) and
551 "during" (lower two panels) conditions. Scale bars, 2 μm. **(C, D)** Quantification of
552 area ratio values at indicated time in "before" (C) or "during" (D) recording.
553 Twenty-nine nuclei (C) and 33 nuclei (D) from 3 independent experiments were
554 analyzed. Data are means +s.d. n.s., not significant (one-way ANOVA followed
555 by Tukey's multiple-comparison test).
556
557
558 **Supplementary figure 1. Expression changes of an IEG upon visual**
559 **stimulation after enucleation, dark rearing, and light exposure.**
560 **(A)** Left eyes of 6- to 9-week-old *ICR* wild-type mice were enucleated, and the
561 mice were harvested in a dark room for five days. They were stimulated by room
562 light for four hours and subjected to Reverse transcription and quantitative
563 polymerase chain reaction (RT-qPCR). **(B)** RT-qPCR analysis of relative *Npas4*
564 mRNA abundance (normalized by the amount of *Gapdh* mRNA) in the primary
565 visual cortex was performed. Data are means ± s.d., averaged values for four
566 mice. *$p < 0.05$ (two-tailed Student's paired t-test).
567
568 **Supplementary figure 2. The changes in the expression level of an IEG after**
569 **MK-801 injection.**
570 **(A)** RT-qPCR analysis of relative *Npas4* mRNA abundance (normalized by the
571 amount of *Gapdh* mRNA) in the primary visual cortex after injection of saline or
572 MK-801 was performed. Data are means ± s.d., averaged values for four mice.
573 *$p < 0.05$ (two-tailed Student's paired t-test).
574

Supplementary Video 1

The nuclear shape of excitatory neurons in the visual cortex of 6- to 9-week-old *Nex-Cre;SUN1-GFP* mouse before stimulation. This video is played at 120× speed.

Supplementary Video 2

The nuclear shape of excitatory neurons in the visual cortex of 6- to 9-week-old *Nex-Cre;SUN1-GFP* mouse during stimulation. This video is played at 120× speed.

Supplementary Video 3

The nuclear shape of excitatory neurons in the visual cortex of 6- to 9-week-old *Nex-Cre;SUN1-GFP* mouse after stimulation. This video is played at 120× speed.

Supplementary Video 4

The nuclear shape of excitatory neurons in the visual cortex of 6- to 9-week-old *Nex-Cre;SUN1-GFP* mouse after MK-801 injection. This video is played at 120× speed.

Supplementary Video 5

The nuclear shape of excitatory neurons in the visual cortex of >98-week-old *Nex-Cre;SUN1-GFP* mouse before stimulation. This video is played at 120× speed.

Supplementary Video 6

The nuclear shape of excitatory neurons in the visual cortex of >98-week-old *Nex-Cre;SUN1-GFP* mouse during stimulation. This video is played at 120× speed.

606 **Supplementary Table 1. Primer sequences for RT-qPCR**

607

Gene	Forward primer	Reverse primer
GAPDH	atgaatacggctacagcaacagg	ctcttgctcagtgtccttgctg
Npas4	ctgtccttgtagtgaactggtta	acaccaagtacagtgacttt
c-Fos	acccttttgatgacttcttgt	gtctgctgcatagaaggaac

608

609

610

611 **Supplementary Table 2. Antibodies for immunohistochemistry.**

612

Antigen	Manufacturer	Serial Number	Concentration
GFP	Abcam	ab13970	1:2000
c-Fos	Santa Cruz	sc-271243	1:100
Lamin B1	Abcam	ab16048	1:250

613

614

References

Alcalá-Vida, R., Garcia-Forn, M., Castany-Pladevall, C., Creus-Muncunill, J., Ito, Y., Blanco, E., Golbano, A., Crespí-Vázquez, K., Parry, A., Slater, G., et al. (2021). Neuron type-specific increase in lamin B1 contributes to nuclear dysfunction in Huntington's disease. Embo Mol Med *13*, e12105. https://doi.org/10.15252/emmm.202012105.

Berardi, N., Pizzorusso, T., and Maffei, L. (2000). Critical periods during sensory development. Curr Opin Neurobiol *10*, 138–145. https://doi.org/10.1016/s0959-4388(99)00047-1.

Chen, X., Xie, C., Tian, W., Sun, L., Zheng, W., Hawes, S., Chang, L., Kung, J., Ding, J., Chen, S., et al. (2020). Parkinson's disease-related Leucine-rich repeat kinase 2 modulates nuclear morphology and genomic stability in striatal projection neurons during aging. Mol Neurodegener *15*, 12. https://doi.org/10.1186/s13024-020-00360-0.

Dana, H., Mohar, B., Sun, Y., Narayan, S., Gordus, A., Hasseman, J.P., Tsegaye, G., Holt, G.T., Hu, A., Walpita, D., et al. (2016). Sensitive red protein calcium indicators for imaging neural activity. Elife *5*, e12727. https://doi.org/10.7554/elife.12727.

Eto, H., Kishi, Y., Yakushiji-Kaminatsui, N., Sugishita, H., Utsunomiya, S., Koseki, H., and Gotoh, Y. (2020). The Polycomb group protein Ring1 regulates dorsoventral patterning of the mouse telencephalon. Nature Communications *11*, 5709. https://doi.org/10.1038/s41467-020-19556-5.

Fernandez-Albert, J., Lipinski, M., Lopez-Cascales, M.T., Rowley, M.J., Martin-Gonzalez, A.M., Blanco, B. del, Corces, V.G., and Barco, A. (2019). Immediate and deferred epigenomic signatures of in vivo neuronal activation in mouse hippocampus. Nat Neurosci *22*, 1718–1730. https://doi.org/10.1038/s41593-019-0476-2.

Feurle, P., Abentung, A., Cera, I., Wahl, N., Ablinger, C., Bucher, M., Stefan, E., Sprenger, S., Teis, D., Fischer, A., et al. (2020). SATB2-LEMD2 interaction links nuclear shape plasticity to regulation of cognition-related genes. The EMBO Journal e103701. https://doi.org/10.15252/embj.2019103701.

Flavell, S.W., and Greenberg, M.E. (2008). Signaling Mechanisms Linking Neuronal Activity to Gene Expression and Plasticity of the Nervous System. Annu Rev Neurosci *31*, 563–590. https://doi.org/10.1146/annurev.neuro.31.060407.125631.

651 Goebbels, S., Bormuth, I., Bode, U., Hermanson, O., Schwab, M.H., and Nave,
652 K. (2006). Genetic targeting of principal neurons in neocortex and hippocampus
653 of NEX-Cre mice. Genesis *44*, 611–621. https://doi.org/10.1002/dvg.20256.

654 Greer, P.L., and Greenberg, M.E. (2008). From synapse to nucleus: calcium-
655 dependent gene transcription in the control of synapse development and
656 function. Neuron *59*, 846–860. https://doi.org/10.1016/j.neuron.2008.09.002.

657 Katz, L.C., and Crowley, J.C. (2002). Development of cortical circuits: Lessons
658 from ocular dominance columns. Nat Rev Neurosci *3*, 34–42.
659 https://doi.org/10.1038/nrn703.

660 Liu, G.-H., Qu, J., Suzuki, K., Nivet, E., Li, M., Montserrat, N., Yi, F., Xu, X.,
661 Ruiz, S., Zhang, W., et al. (2012). Progressive degeneration of human neural
662 stem cells caused by pathogenic LRRK2. Nature *491*, 603–607.
663 https://doi.org/10.1038/nature11557.

664 Lyckman, A.W., Horng, S., Leamey, C.A., Tropea, D., Watakabe, A., Wart, A.V.,
665 McCurry, C., Yamamori, T., and Sur, M. (2008). Gene expression patterns in
666 visual cortex during the critical period: synaptic stabilization and reversal by
667 visual deprivation. Proceedings of the National Academy of Sciences *105*,
668 9409–9414. https://doi.org/10.1073/pnas.0710172105.

669 Mo, A., Mukamel, E.A., Davis, F.P., Luo, C., Henry, G.L., Picard, S., Urich,
670 M.A., Nery, J.R., Sejnowski, T.J., Lister, R., et al. (2015). Epigenomic
671 Signatures of Neuronal Diversity in the Mammalian Brain. Neuron *86*, 1369–
672 1384. https://doi.org/10.1016/j.neuron.2015.05.018.

673 Murakami, T., Yoshida, T., Matsui, T., and Ohki, K. (2015). Wide-field Ca2+
674 imaging reveals visually evoked activity in the retrosplenial area. Front Mol
675 Neurosci *08*, 20. https://doi.org/10.3389/fnmol.2015.00020.

676 Noguchi, A., Ito, K., Uosaki, Y., Ideta-Otsuka, M., Igarashi, K., Nakashima, H.,
677 Kakizaki, T., Kaneda, R., Uosaki, H., Yanagawa, Y., et al. (2021). Decreased
678 Lamin B1 Levels Affect Gene Positioning and Expression in Postmitotic
679 Neurons. Neurosci Res *173*, 22–33.
680 https://doi.org/10.1016/j.neures.2021.05.011.

681 Ohki, K., and Reid, R.C. (2014). In Vivo Two-Photon Calcium Imaging in the
682 Visual System. Cold Spring Harb Protoc *2014*, pdb.prot081455.
683 https://doi.org/10.1101/pdb.prot081455.

684 Pajerowski, J.D., Dahl, K.N., Zhong, F.L., Sammak, P.J., and Discher, D.E.
685 (2007). Physical plasticity of the nucleus in stem cell differentiation.
686 Proceedings of the National Academy of Sciences of the United States of
687 America *104*, 15619–15624. https://doi.org/10.1073/pnas.0702576104.

Shani, V., Safory, H., Szargel, R., Wang, N., Cohen, T., Elghani, F.A., Hamza, H., Savyon, M., Radzishevsky, I., Shaulov, L., et al. (2019). Physiological and pathological roles of LRRK2 in the nuclear envelope integrity. Hum Mol Genet *28*, 3982–3996. https://doi.org/10.1093/hmg/ddz245.

Tyssowski, K.M., DeStefino, N.R., Cho, J.-H., Dunn, C.J., Poston, R.G., Carty, C.E., Jones, R.D., Chang, S.M., Romeo, P., Wurzelmann, M.K., et al. (2018). Different Neuronal Activity Patterns Induce Different Gene Expression Programs. Neuron *98*, 530-546.e11. https://doi.org/10.1016/j.neuron.2018.04.001.

Wittmann, M., Queisser, G., Eder, A., Wiegert, J.S., Bengtson, C.P., Hellwig, A., Wittum, G., and Bading, H. (2009). Synaptic activity induces dramatic changes in the geometry of the cell nucleus: interplay between nuclear structure, histone H3 phosphorylation, and nuclear calcium signaling. Journal of Neuroscience *29*, 14687–14700. https://doi.org/10.1523/jneurosci.1160-09.2009.

Wong, R.O.L., and Ghosh, A. (2002). Activity-dependent regulation of dendritic growth and patterning. Nature Reviews Neuroscience *3*, 803–812. https://doi.org/10.1038/nrn941.

Figure 1, Frey et al.

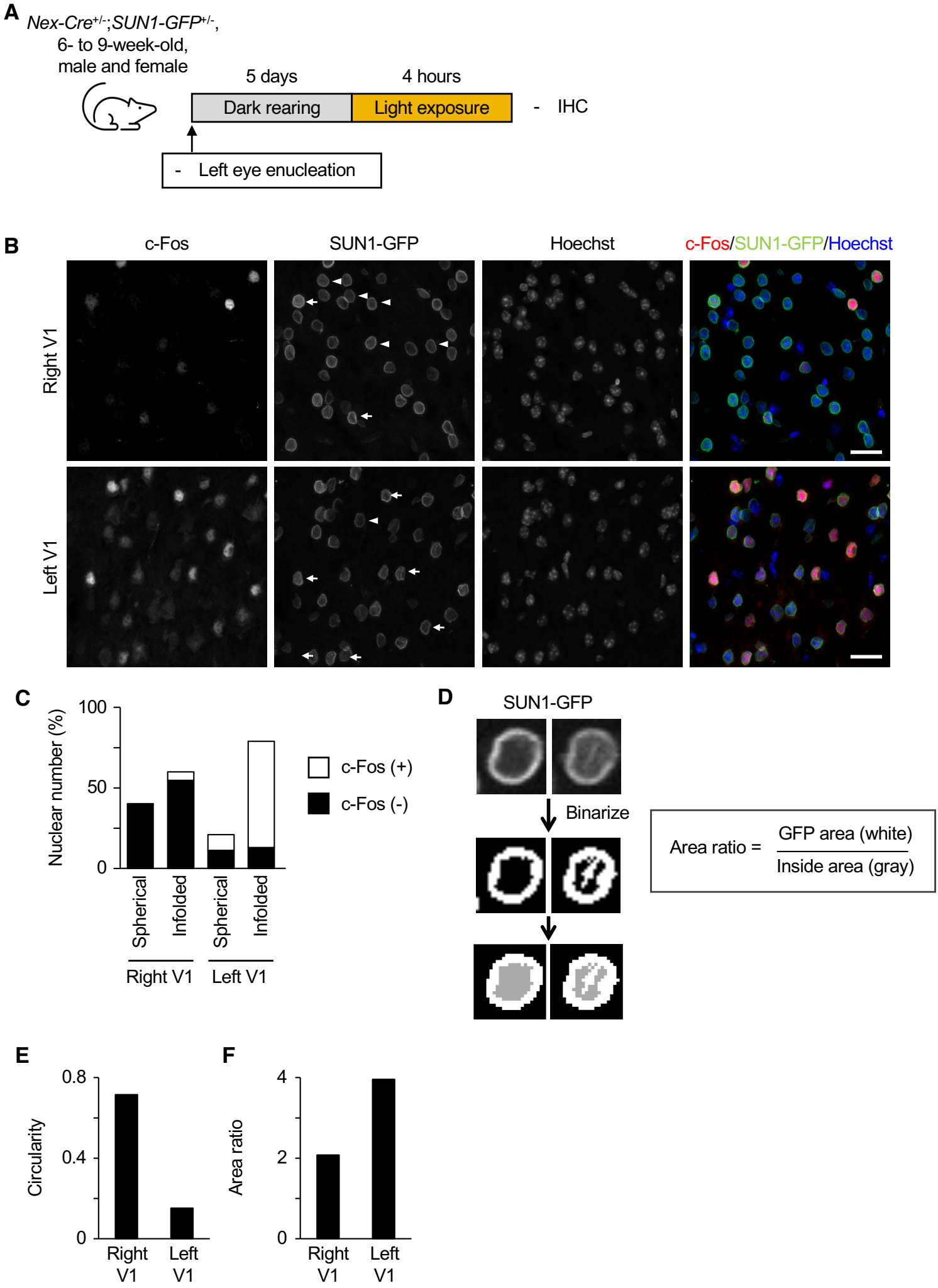

Figure 2, Frey et al.

A

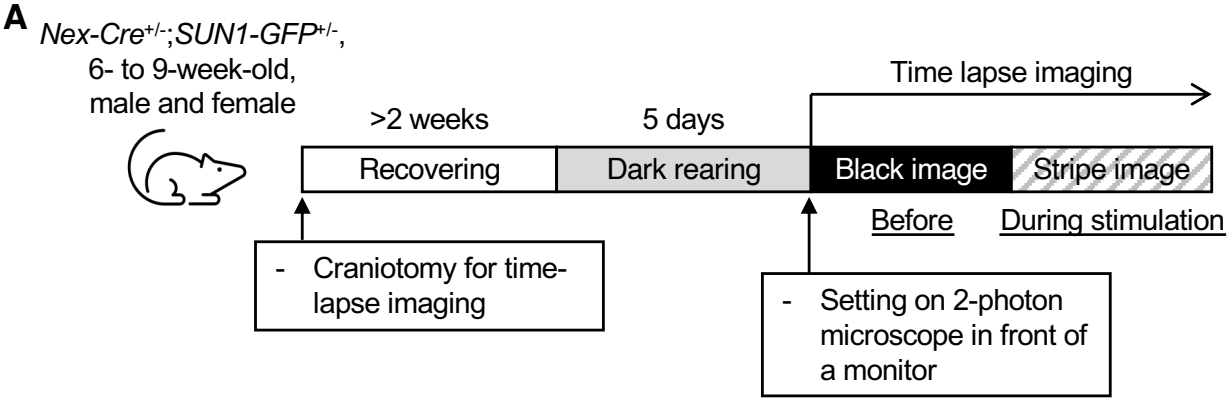

B

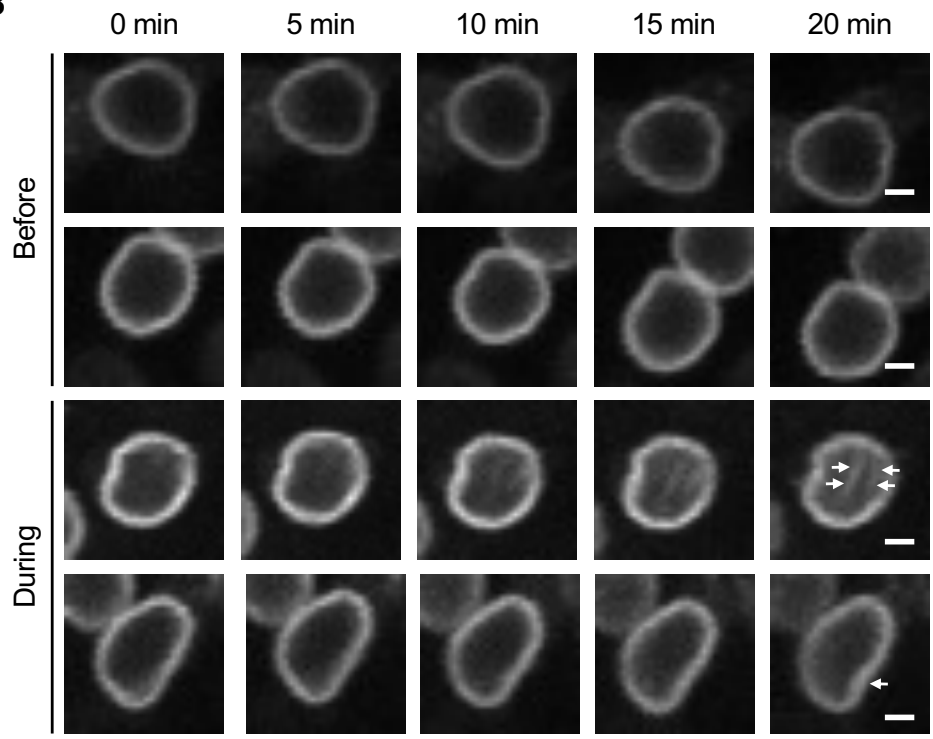

C

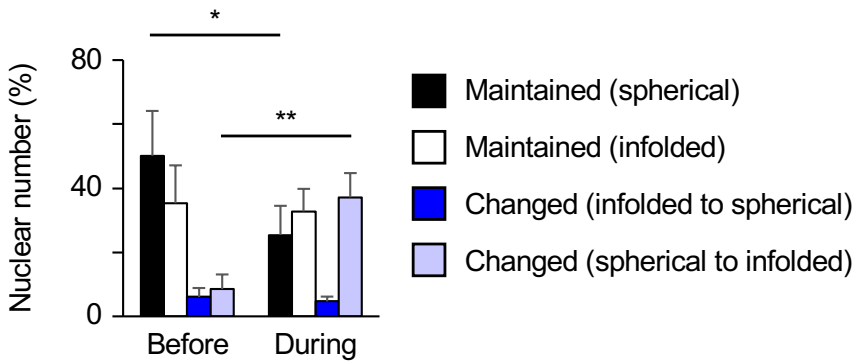

Figure 3, Frey et al.

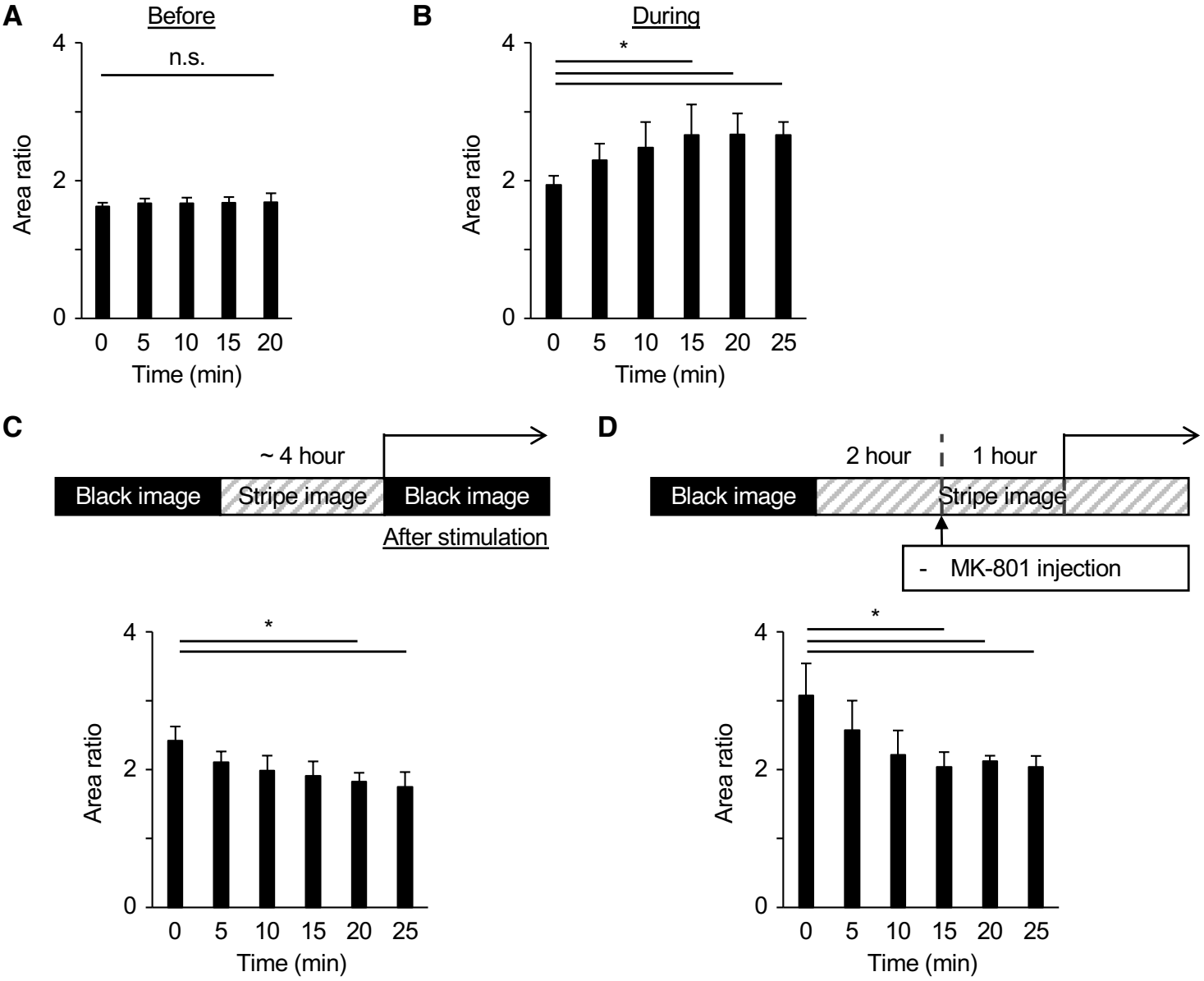

Figure 4, Frey et al.

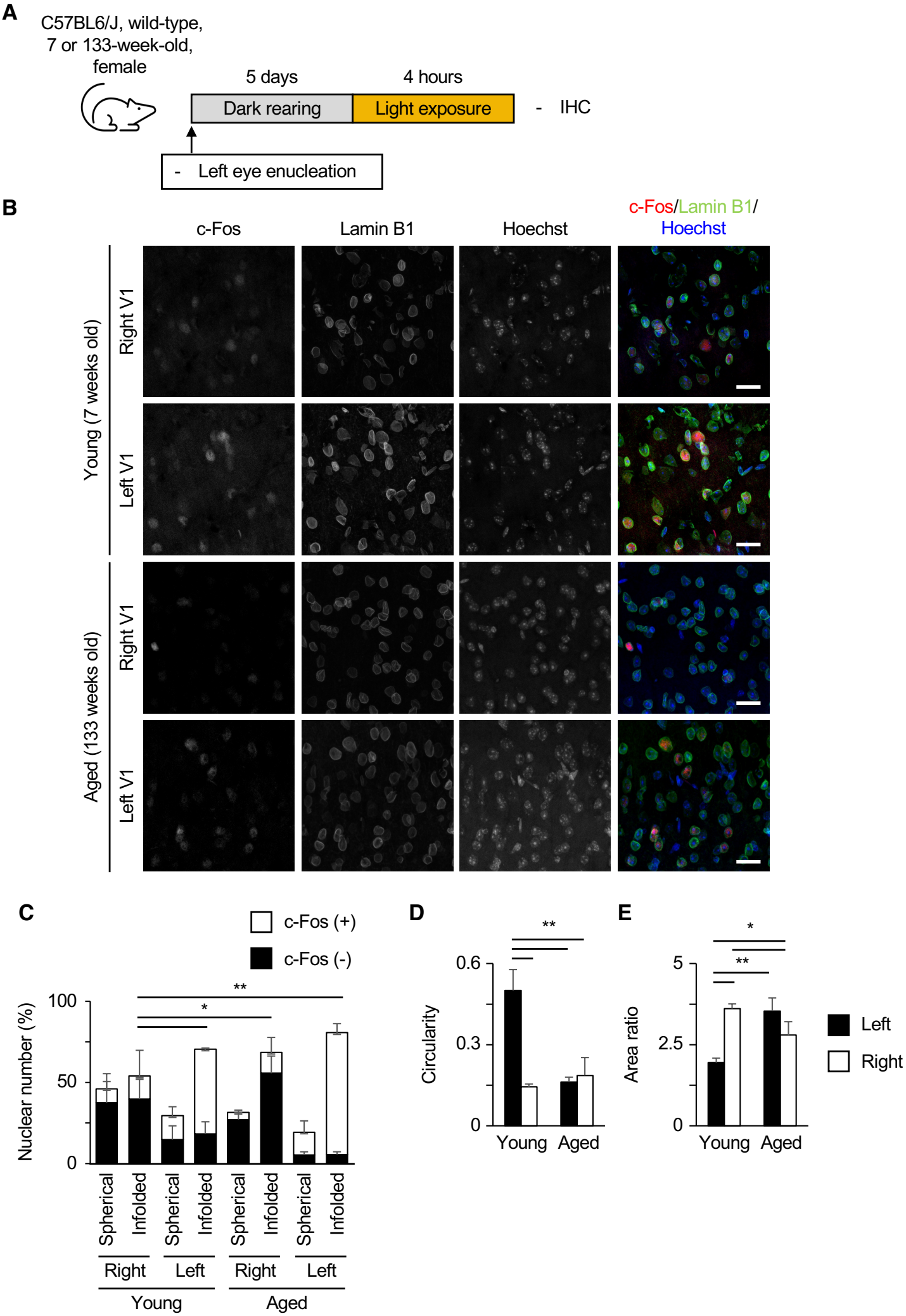

Figure 5, Frey et al.

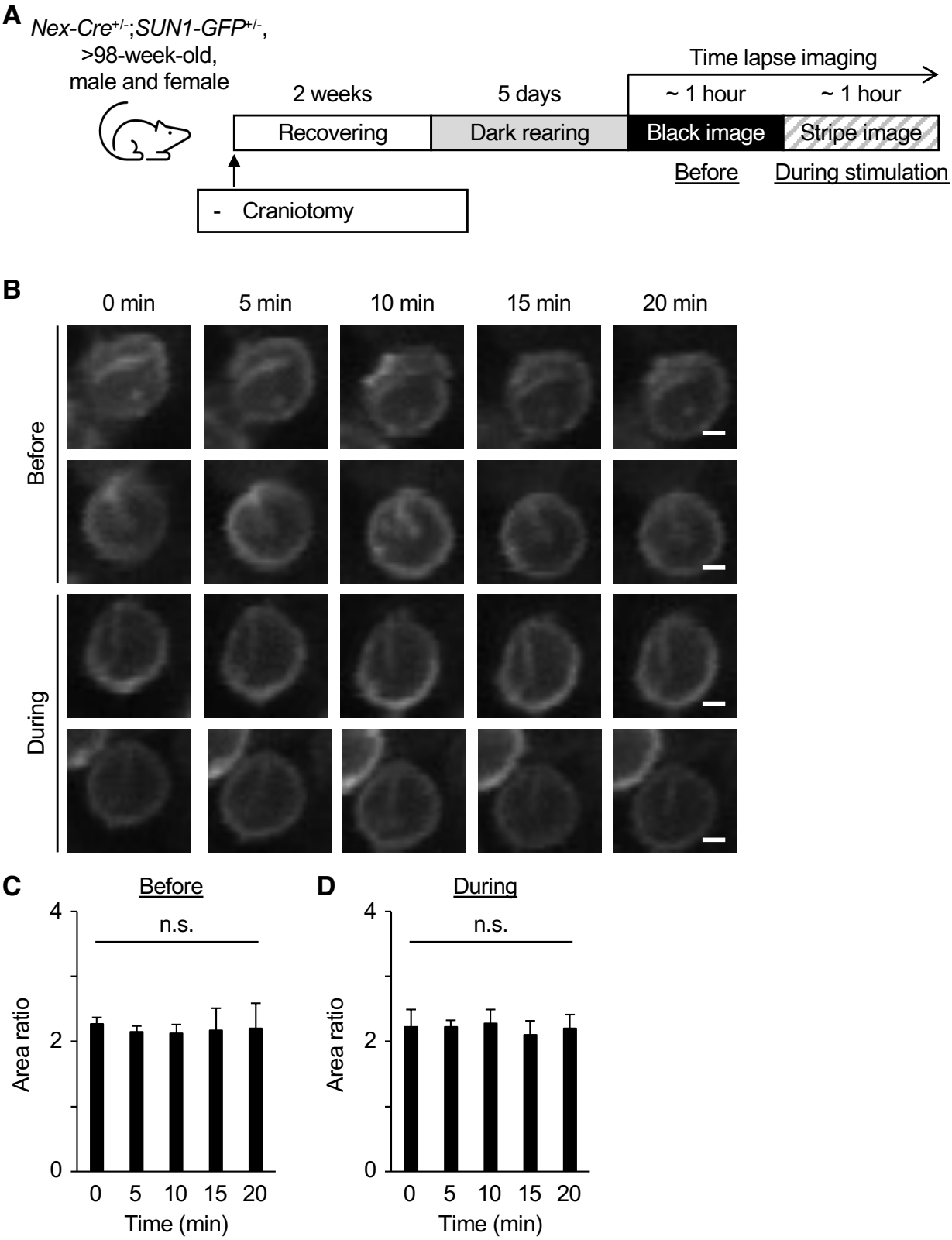

Supplementary figure 1, Frey et al.

A

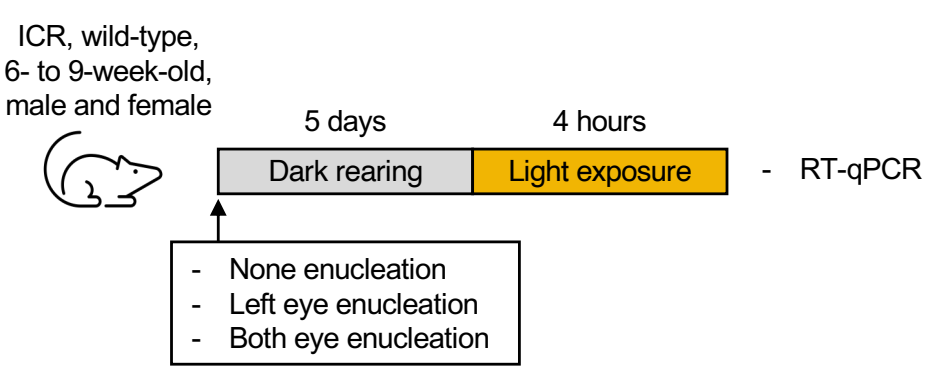

B

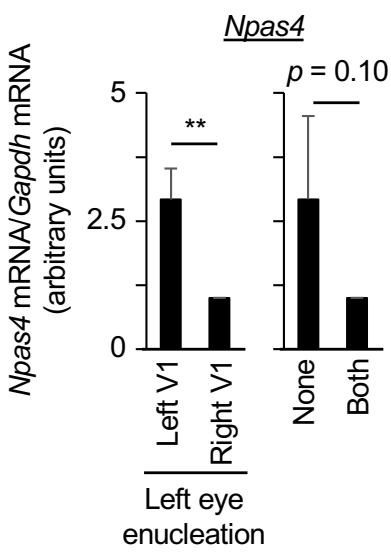

Supplementary figure 2, Frey et al.
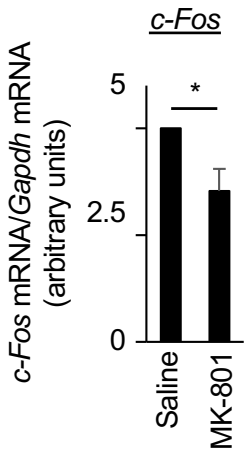
A